Article:

Miao, H. orcid.org/0000-0003-2982-2465, Xu, H., Yang, K. et al. (5 more authors) (2025) The reversal of surface wind speed trend in Northeast China: impact from aerosol emissions. Climate Dynamics, 63 (1). 43. ISSN 0930-7575

https://doi.org/10.1007/s00382-024-07544-0

The reversal of surface wind speed trend in Northeast China: impact from aerosol emissions

Haozeyu Miao[1,2], Haiming Xu[1,2*], Kai Yang[6], Haosu Tang[3], Jiechun Deng[1,2], Meng Xu[1,2], Guicai Ning[7] and Gang Huang[4,5]

[1] Key Laboratory of Meteorological Disaster (KLME), Ministry of Education & Collaborative Innovation Center on Forecast and Evaluation of Meteorological Disasters (CIC-FEMD), Nanjing University of Information Science & Technology, Nanjing, People's Republic of China

[2] School of Atmospheric Sciences, Nanjing University of Information Science & Technology, Nanjing, People's Republic of China

[3] Department of Geography, University of Sheffield, Sheffield, UK

[4] Laboratory for Regional Oceanography and Numerical Modeling, Qingdao National Laboratory for Marine Science and Technology, Qingdao, People's Republic of China

[5] University of Chinese Academy of Sciences, Beijing, People's Republic of China

[6] Center for Southern Hemisphere Oceans Research (CSHOR), CSIRO Oceans and Atmosphere, Hobart, TAS, Australia

[7] School of Atmospheric Physics, Nanjing University of Information Science & Technology, Nanjing, People's Republic of China

*Corresponding author: Prof. Haiming Xu (E-mail: hxu@nuist.edu.cn)

Abstract

A "stilling" or "reversal" of surface wind speed (SWS) trend over the landmass of the Northern Hemisphere has been observed during the past decades, with notable regional disparities. The mechanism behind such change in SWS trend in each region is inadequately understood. This study focuses on the interdecadal variation of SWS in Northeast China from 1980 to 2020, revealing a reversal of SWS trend since 2010 with a decreasing trend before 2010 and an obvious increasing trend thereafter. This reversal is primarily attributed to an interdecadal decline in local aerosols measured by aerosol optical depth (AOD), which decreases low-level static stability and enhances turbulent kinetic energy (TKE), thus increasing local SWS. This finding is supported by a significant negative correlation between AOD and SWS in the aerosol-only forcing experiment from the Detection and Attribution Model Intercomparison Project (DAMIP). Quantitative analyses further confirm that the anthropogenic aerosol reduction is the dominant contributor to the increasing SWS observed in the recent decade. Mid-term and long-term projected SWS exhibits the fastest drop under SSP3-7.0 scenario, which represents the highest aerosol emissions. These findings emphasize the importance of considering aerosol changes for a comprehensive understanding of SWS changes on regional scales.

Key words

Wind speed reversal, aerosol, CMIP6, Northeast China, attribution, future projection

1. Introduction

Under the background of global warming, the global surface wind speed (SWS) has been generally reduced over land, known as the SWS "stilling" (Tian *et al* 2019, Vautard *et al* 2010). Particularly, the SWS decline is also reported in China, which is the largest market of global wind energy (Guo *et al* 2011, Lin *et al* 2013). The weakening of SWS is not only related to the internal variability associated with atmospheric circulation, but also comes from the impact of human activities such as land use and land cover change (LUCC), greenhouse gas (GHG) emission, and anthropogenic aerosols. For example, Xu *et al* (2006) suggested that the decrease in SWS over China from 1969 to 2000 was due to the steady decline in the East Asian monsoon. Fast warming helps weaken the annual and seasonal mean meridional air temperature gradients, which contribute to the slowdown of winds over northern China (Zhang *et al* 2021). Based on the observation minus reanalysis (OMR) method, Zha *et al* (2017) quantified the effects of LUCC on SWS and found that LUCC can account for a downward trend of -0.12 m s^{-1} per decade in SWS in China over the last 30 years. As an important atmosphere component, aerosol can induce global and regional climate responses in different ways. Previous studies indicated that the variation of aerosol optical depth (AOD) had significant influences on various near-surface meteorological variables, such as vegetation and precipitation (Li *et al* 2011, Taric *et al* 2022). In terms of aerosol impact on SWS, Jacobson and Kaufman (2006) suggested that aerosol particles may weaken the short-term SWS in California by stabilizing the atmosphere. Bichet *et al* (2012) reported a decline of -0.3 m s^{-1} in global terrestrial SWS from 1975 to 2005, which is related to the increasing aerosol emissions based on sensitivity experiments.

Despite the generally decreasing SWS trend, several studies have reported SWS reversal over land during the past decade (Zeng *et al* 2019, Zha *et al* 2021b). However, notable disparities exist in the reversal timing of SWS trend due to the use of different datasets, regions, and periods. For example, the SWS reversals in North America, Europe, and Asia occurred in 2012, 2003, and 2001, respectively (Zeng *et al* 2019).

Zhang and Wang (2020) divided the SWS trends in China from 1960 to 2017 into three periods, and found a near-zero annual trend from 1960 to 1969, a prominent decrease of -0.24 m s^{-1} per decade from 1970 to 2004, and a weak reversal from 2005 to 2017. Ge *et al* (2021) reported that after two decades of sharp declines at a rate of 0.172 m s^{-1} per decade, the SWS over Northwest China began to increase significantly at a rate of 0.065 m s^{-1} per decade since 2003. Using the observations at 110 stations in Southwest China, Yang *et al* (2012) found SWS recovery occurred in 2000. Different SWS reversal features underscore the presence of distinct factors controlling the SWS trend in each area. Previous studies generally attributed the reversal of SWS trend in China to large-scale ocean-atmosphere circulation (LOAC) signals, such as the Arctic Oscillation (AO) and Pacific Decadal Oscillation (PDO) (Li *et al* 2022, Zha *et al* 2021b).

The influences of various external forcing factors, including GHGs, aerosols from industrial activities and biomass burning, and LUCC, in modifying regional SWS changes, however, have not been thoroughly investigated. In particular, the joint or competing impacts of GHGs and aerosols on the spatiotemporal patterns of regional SWS changes have yet to be quantified. Here, we show that the characteristic of SWS reversal over Northeast China differs from that in the other regions of China. By examining the historical SWS change in Northeast China, we highlight the potential impact from recent aerosol reduction. This study may fill research gaps and deepen our understanding of long-term SWS variation. The remainder of the paper is structured as follows. In Section 2, we describe the datasets and methods used in this study. In Section 3, we explore the observed evolution of SWS in Northeast China and a likely mechanism behind this interdecadal change, and we also give future projections of SWS under different scenarios. We conclude the paper with some discussion in Section 4.

2. Data and methods

2.1. Data

2.1.1. SWS observations

We use daily SWS data observed from ground weather stations from 1980 to 2020 to calculate monthly averaged SWS field across China. The stations are carefully selected from the China Meteorological Administration (CMA) database based on strict quality control procedures, such as the temporal consistency test, homogeneity test, and extreme test. We use the Pettitt test (Pettitt 1979) to retain the stations without any change point. Finally, 157 stations with continuous monthly wind records in Northeast China are retained for the study period of 1980-2020 (Figure 1a).

2.1.2. Reanalysis datasets

In this study, the monthly mean AOD at 550 nm is obtained from the Modern Era Retrospective analysis for Research and Applications Version 2 (MERRA-2) provided by the National Aeronautics and Space Administration (NASA). The data is on 72 vertical levels at a resolution of 0.5°×0.625° (Gelaro *et al* 2017).

Considering inherent limitations in reanalysis datasets, we compare observed SWS with those from four different reanalysis datasets, including the fifth generation European Centre for Medium-Range Weather Forecasts (ECMWF) reanalysis (ERA-5) on 60 vertical levels with a resolution of 0.125° (Hersbach *et al* 2020), the Japanese Meteorological Agency 55-Year Reanalysis (JRA-55) on 37 vertical levels with a resolution of 1.25° (Kobayashi *et al* 2015), the National Centers for Environmental Prediction (NCEP) Climate Forecast System Reanalysis (CFSR) on 64 vertical levels with a resolution of 0.5° (Saha *et al* 2010), and MERRA-2. All reanalysis datasets are widely used for climate change studies across China (Jiang *et al* 2021, Miao *et al* 2020, Su *et al* 2015).

2.1.3. Model outputs

To validate SWS responses to AOD variation, we also use simulations from the Detection and Attribution Model Intercomparison Project (DAMIP; Gillett *et al* 2016) in the Coupled Model Intercomparison Project Phase 6 (CMIP6). The DAMIP simulations are single-forcing experiments (with only one external forcing of interest varying over time and all other forcings keeping at the constant pre-industrial levels). The experiments used in this paper are hist-aer (with anthropogenic aerosol forcing only; referred to as AER), hist-GHG (with well-mixed GHG forcing only; referred to as GHG), and hist-nat (with natural forcing only; i.e., volcanic and solar activities; referred to as NAT). The selected variables include monthly near-surface wind speed, aerosol optical thickness at 550 nm, and air temperature from 1000 to 850 hPa with an interval of 75 hPa. We use eight models with the mentioned experiments and variables covering the historical period of 1900-2020, with three realizations using for each model and each scenario. Multi-model ensemble (MME) means are used to determine which forcing factor is responsible for different responses in the historical experiments.

For future projections, four typical emission scenarios under the Shared Socioeconomic Pathways (SSPs; O'Neill *et al* 2016) are considered in this study, including SSP1-2.6, SSP2-4.5, SSP3-7.0, and SSP5-8.5, which are driven by different anthropogenic emissions. The models and the realizations used in historical experiments and the Scenario Model Intercomparison Project (ScenarioMIP) are the same as those in the DAMIP, except for HadGEM3-GC31-LL, which lacks the simulations under the SSP3-7.0 scenario. The list of models included in each set of simulations can be found in Table S1 in the Supporting Information. To facilitate inter-model comparison, all model outputs are remapped onto a 1°×1° grid using bilinear interpolation (Miao *et al* 2023).

2.2. Methods

2.2.1. Definition of static stability

Atmospheric static stability measures the gravitational resistance of the atmosphere to vertical displacement, which reflects the characteristics of the atmosphere affecting the vertical motion. It is the result of a fundamental adjustment of buoyancy, and thus is determined by the vertical stratification of potential temperature or density. The following equation is used to calculate the static stability (Bluestein 1992):

$$S = -\frac{T}{\theta} \times \frac{d\theta}{dP}$$

where *T* is the air temperature, *θ* is the potential temperature, and *P* is the pressure. The static stability influences the dynamics of various atmospheric motions including wind.

2.2.2. Statistical methods

For consistency, all variables cover the same study period of 1980-2020. The Mann-Kendall test for trend in Sen's slope estimate (Sen 1968) is used to detect trends in SWS and to estimate trend magnitude and its significance. The method does not assume a particular distribution of the data and is not sensitive to outliers. This statistical significance test for trends may not be reliable for the highly auto-correlated time series. Fourier analysis and Gaussian filtering are performed to remove interannual variation (Schaefer and Domroes 2009, Moreira *et al* 2015) with a focus on interdecadal variation.

2.2.3. Multiple linear regression model

To quantitatively decompose the contributions of AER, GHG, and NAT forcing factors to observed SWS changes, we construct a combined index using a multiple linear regression model, which is represented as follows:

$$SWS_{OBS} = a \times SWS_{AER} + b \times SWS_{GHG} + c \times SWS_{NAT} + d$$

In this model, SWS_{OBS} denotes observed SWS change, while SWS_{AER}, SWS_{GHG}, and SWS_{NAT} represent the contributions from aerosol, GHG, and natural forcings, respectively. The coefficients *a*, *b*, and *c* quantify the relative impacts of the respective forcing factors; and *d* represents the intercept term that captures any constant bias in the observation data. This approach allows us to isolate individual effects of different forcing factors on the overall SWS change.

3. Results

3.1. Observed changes in the SWS and AOD over Northeast China

The raw and interdecadal variations of the SWS and AOD time series over Northeast China are shown in Figure 1b. The correlation of interdecadal variations between SWS and AOD reaches -0.80 ($P < 0.001$), indicating that the epochs with higher SWS correspond to those with lower aerosol emissions. Simultaneous reversals of the interdecadal SWS and AOD are observed around 2010, with a significant trend shift preceding and following this year. During 1980-2020, the SWS over Northeast China exhibits negative and positive trends before and after 2010, while the corresponding AOD shows the opposite trends. The trend of SWS is -0.214 m s^{-1} per decade ($P < 0.001$) during 1980-2010 and 0.467 m s^{-1} per decade ($P < 0.01$) during 2010-2020. For the AOD, the trends are 0.023 per decade ($P < 0.05$) and -0.086 per decade ($P < 0.05$) for the two periods before and after 2010, respectively. Seasonally, the interdecadal evolution of SWS is generally consistent with that of the annual mean, transitioning from a negative to a positive trend around year 2010 (Figure S1). The seasonal interdecadal correlation coefficient between SWS and AOD is as follows: -0.86 in spring ($P < 0.001$), -0.87 in summer ($P < 0.001$), -0.61 in autumn ($P < 0.05$), and -0.50 in winter ($P < 0.05$). There are some seasonal differences in AOD evolution, with spring and summer AOD peaking in 2010 and declining thereafter, consistent with its annual mean. The AOD reversal lags slightly in autumn, while the trend shift is less pronounced in winter. These are due to the fact that anthropogenic aerosol emissions are concentrated in spring and summer, with lower values in autumn and winter. The climatological means for the four seasons of spring, summer, autumn, and winter are 0.36, 0.35, 0.24, and 0.20, respectively. These results are consistent with previous findings that the AOD over East Asia reaches its maximum in spring and its minimum in winter (Bao *et al* 2009, He *et al* 2012, Kim *et al* 2007).

The SWS reversal over Northeast China does not imply that SWS exhibits increasing trends at all the stations used. To rule out the possibility that the reversal is solely driven by significant changes in SWS at a few stations, we show spatial patterns of the SWS trends for 2000-2010 and 2010-2020 in Figures 1c and 1d, respectively. We can see that 75.6% of the total stations (90 out of the 119 stations) display significant decreasing SWS trends before 2010 ($P < 0.1$). Conversely, after 2010, 96.2% of the total stations (102 out of the 106 stations) present mean annual SWS with increasing trends at $P < 0.1$ level. The spatial contrast in AOD changes is more pronounced, with the increasing trend in the early period and the decreasing trend in the late period for almost all the stations (Figures 1e and 1f). The spatial trends of seasonal SWS are consistent, that is, 86.2%, 83.2%, 73.3%, and 61.7% of all the stations show decreasing trends in spring, summer, autumn, and winter from 2000-2010 at $P < 0.1$ level (Figure S2). These percentages increase to 93.1%, 99.1%, 96.4%, and 91.0%, respectively, after 2010 at $P < 0.1$ level, indicating a robust reversal of the SWS in Northeast China. In addition, the AOD at almost all stations shows opposite trend changes in the periods before and after 2010, with trend values more pronounced in spring and summer than in the other seasons (Figure S3).

Since the annual mean variabilities of SWS and AOD show the main features of their intra-annual cycles, we will focus on the annual mean timescale next.

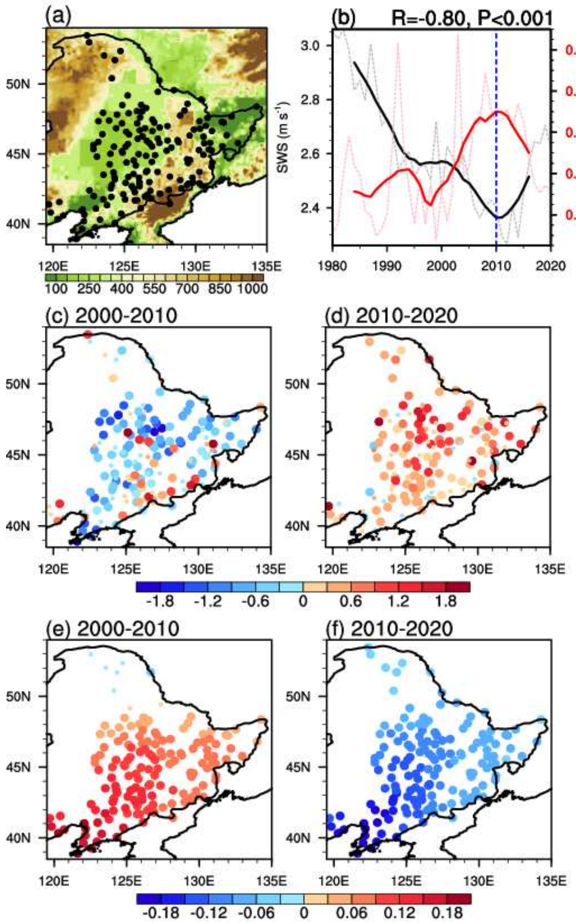

Figure 1. (**a**) Geographic distribution and terrain heights (units: m) of the 157 meteorological stations in Northeast China. (**b**) Time series of raw (light dashed curve) and 9-year Gaussian low-pass filtered (heavy solid curve) observed SWS (black; units: m s^{-1}) and AOD (red) at 550 nm in Northeast China from 1980 to 2020. The vertical dashed blue line denotes the turning point in year 2010. Spatial patterns of linear trends in SWS (**c** and **d**; units: m s^{-1} per decade) and AOD (**e** and **f**; units: per decade) during the two periods of 2000-2010 (**c** and **e**) and 2010-2020 (**d** and **f**) are shown. Larger dots in (**c**-**f**) indicate the 90% confidence level (i.e., $P < 0.1$).

3.2. Potential mechanisms between SWS and AOD shifts

Before exploring the possible effects of AOD on SWS variation, we assess the capability of the reanalysis datasets in reproducing long-term changes in SWS trend (Figure S4). Except for the ERA-5, all reanalysis datasets can reproduce the SWS reversal in Northeast China, although the SWS reversals in the CFSR and MERRA-2 lag slightly behind those in the observations. Note that the trend magnitudes of different reanalysis datasets differ, and all of them tend to underestimate the trends both before and after the turning point. Consistent with the finding of Miao *et al* (2020) for East Asia, the reanalysis datasets closest to the observations over Northeast China are the JRA-55 and CFSR, which are chosen for the subsequent analyses. Monthly mean air temperatures from the JRA-55 are used to compute the static stability; and monthly mean TKE from the CFSR is also used.

Aerosols interact strongly with meteorological variables within the planetary boundary layer (PBL) and bring about a range of climatic responses (Ding *et al* 2016, Yu *et al* 2002). By scattering and absorbing solar radiation, aerosols can induce temperature inversions, and the resulting strong contrast between surface cooling and upper PBL warming helps stabilize the PBL and attenuate turbulent mixing, thereby reducing SWS. Figures 2a and 2b show the spatial patterns of meridionally averaged atmospheric static stability trends for the two periods before and after 2010, respectively. The trend of the upper-level PBL (above 925 hPa) during the early period is opposite to that of the lower-level PBL (below 925 hPa). This is mainly due to the distinct effects of aerosol absorption on the atmospheric stability of the upper and lower layers. Figure 1a shows that the meteorological stations in Northeast China are mainly located below 925 hPa, corresponding to a general increase in static stability below 925 hPa from 2000 to 2010 (Figure 2a), and a resulting decrease in SWS. This pattern reveals that aerosols cool the surface more rapidly than the upper levels, reducing the vertical temperature gradient and stabilizing the lower atmosphere. In contrast, the decreasing trend in static stability below 925 hPa over the period of 2010-2020 is due to a decrease in aerosols, leading to diminished cooling of the lower layers and thereby enhancing instability (Figure 2b). This is consistent with the hypothesis that SWS generally decreases at plain stations while increases at neighboring hilltop stations, with the largest difference observing around noon due to stronger aerosol radiative effects, indicating trends of stabilization within the PBL and instability above the PBL (Yang *et al* 2013).

The mean altitude of the meteorological stations in Northeast China shown in Figure 1a is 304.7 m, which is close to 975 hPa (about 320 m). To further quantify and understand the relative changes associated with static stability transition, we show the time series of SWS and static stability at 975 hPa (the closest to site-mean altitude) in Figure 2c. The interdecadal static stability exhibits a sharp fluctuating upward trend from 1980 to 2010, and flattens out after 2010. The correlation coefficient between SWS and static stability is -0.98 ($P < 0.001$), revealing that interdecadal variation of static stability is the main cause for the SWS reversal. Figure 2d shows the evolutions of SWS and TKE in the CFSR. The interdecadal correlation between the two variables reaches 0.94 ($P < 0.001$), and is accompanied by a slightly lagged inversion. This suggests that increased aerosol-induced stability suppresses TKE production, consistent with the finding that weak AOD contributes to PBL turbulence growth (Grabowski *et al* 2015, Jiang *et al* 2002). The weakening of turbulence reduces vertical mixing, which in turn reduces the vertical flux of horizontal momentum. Since winds aloft are typically stronger than those near the surface, the weakened vertical mixing reduces the transmission of fast winds aloft to the surface, thus slowing down the SWS.

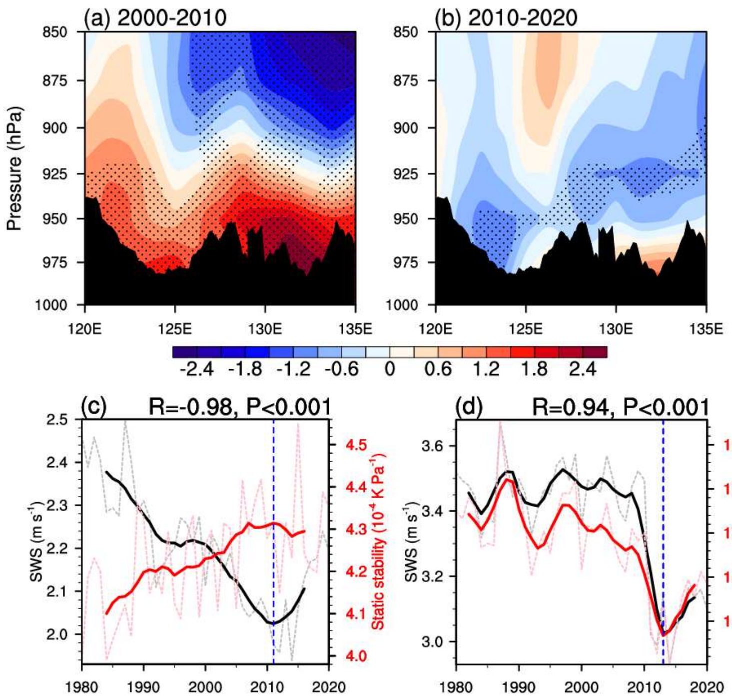

Figure 2. Spatial patterns of linear trends in meridionally averaged static stability (units: 10^{-5} K Pa^{-1} per decade) between 38.5°N and 54°N during the periods of (**a**) 2000-2010 and (**b**) 2010-2020. Stippling in (**a-b**) indicates the significant trend exceeding the 90% confidence level ($P < 0.1$). Topography is indicated by black shading. (**c**) Time series of raw (light dashed curve) and 9-year Gaussian low-pass filtered (heavy solid curve) JRA-55 SWS (black; units: m s^{-1}) and static stability (red; units: 10^{-4} K Pa^{-1}) at 975 hPa in Northeast China from 1980 to 2020. (**d**) Time series of raw (light dashed curve) and 5-year Gaussian low-pass filtered (heavy solid curve) CFSR SWS (black;

units: m s^{-1}) and TKE (red; units: J kg^{-1}) in Northeast China from 1980 to 2020. The vertical dashed blue line in (**c**) and (**d**) denotes the respective turning point.

3.3. Individual effect and quantitative contribution of aerosols, GHG and natural forcing

The DAMIP is widely used to reveal the factors inducing long-term variability in various variables (Shen *et al* 2021, Zhang *et al* 2024). The potential effects of AOD in causing SWS changes are detected based on numerical simulations from the eight DAMIP models of the CMIP6. Temporal evolutions of SWS, AOD, and static stability in the aerosol-only forcing experiment are shown in Figure 3. The changes in AOD are highly consistent across all the models, with sharp increases in AOD since 1940 due to rapid industrialization and urbanization. The AOD peaks in 2010 and has declined dramatically since then as the consequence of clean air actions, which is the same as the observations. We calculate the regional mean static stability at 1000 hPa (closest to the mean terrain height in Northeast China). The static stability of all the models, except for MIROC6 and NorESM2-LM, peaks in 2010 and then decreases, which is similar to the evolution of the AOD. The positive correlation between static stability and the AOD in the MME reaches 0.92 ($P < 0.001$). The SWS shows no significant trend during 1900-1970, while it declines significantly from 1970 to 2010 and increases after 2010 in the MME. The correlation coefficients of SWS with AOD and static stability are -0.95 ($P < 0.001$) and -0.92 ($P < 0.001$), respectively, in the MME, which confirm the observational result that AOD weakens SWS by increasing stability.

Figures 4a-4i display the temporal variations of SWS under different forcing factors. In the GHG-only forcing experiment, the MME result shows fluctuating downward trends in SWS during 1970-2020. This confirms that global warming mainly leads to a decrease in SWS over the Northern Hemisphere (Zha *et al* 2021a), where the Hadley, Ferrell, and Polar cells may be inhibited by substantial GHG warming. Compared to the contribution of GHG, the decreasing trend in SWS due to increasing aerosols is stronger in 1970-2010. The SWS has rebounded rapidly since 2010 when the aerosol begins to decrease, indicating that the SWS change is more sensitive to aerosols than to GHG. However, in the natural-only forcing experiment, there is no significant trend change in SWS in each model over the entire study period of 1900-2020. Using linear regression method, we obtain attributable trends in SWS over 1980-2010 and 2010-2020 (Figures 4j and 4k). Results show that the observed decrease and increase in SWS over Northeast China can be largely explained by AER influence on the basis of the MME responses. During 1980-2010, the trend of aerosol-induced SWS is -0.192 m s^{-1} per decade, accounting for 89.6% of the observed trend. During 2010-2020, the increasing trend of SWS caused by aerosols (0.497 m s^{-1} per decade) even exceeds the observed trend (0.467 m s^{-1} per decade). The influences of GHG and NAT are much weaker over the two periods.

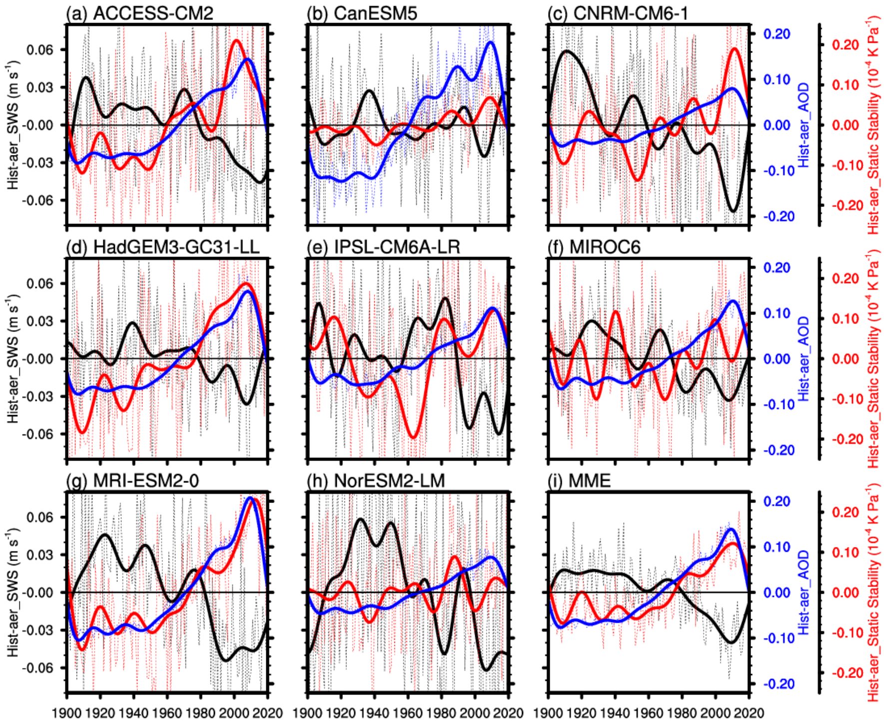

Figure 3. Time series of raw (dashed curve) and 21-year Fourier low-pass filtered (solid curve) anomalies in SWS (black; units: m s^{-1}), AOD (blue), and static stability at 1000 hPa (red; units: 10^{-4} K Pa^{-1}) in the hist-aer (AER) simulation from eight CMIP6 models (**a-h**) and their MME (**i**) during 1900-2020. Each variable is calculated as a regional average for the study area (38.5°-54°N, 119.5°-135°E).

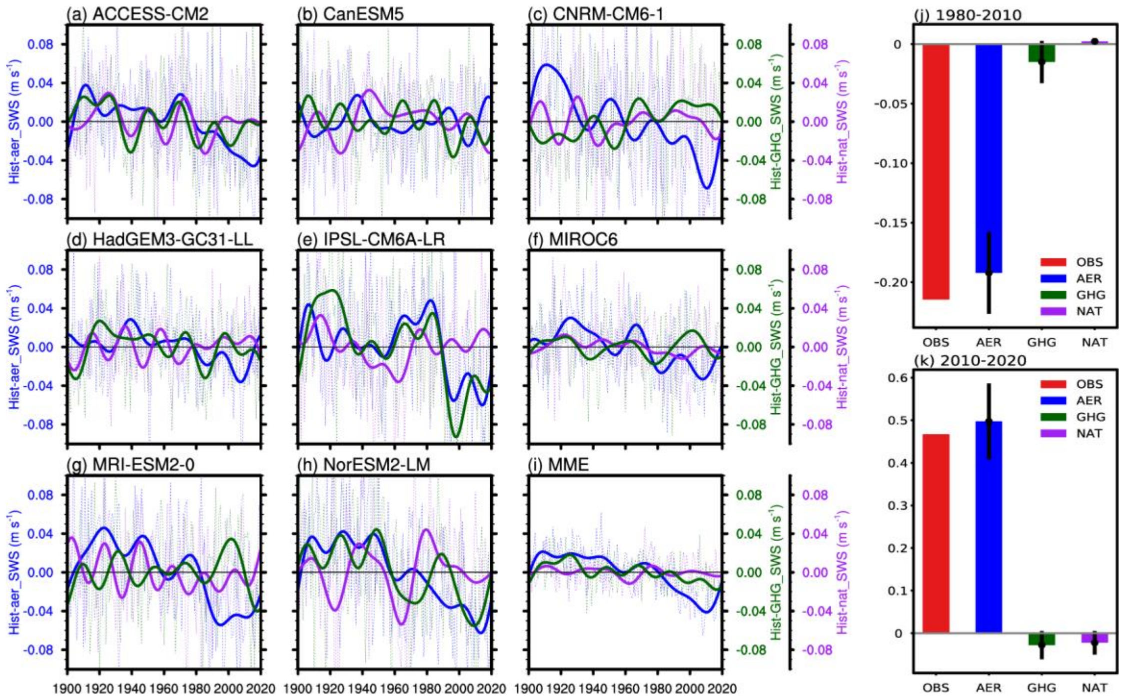

Figure 4. Time series of raw (dashed curve) and 21-year Fourier low-pass filtered (solid curve) SWS anomalies (units: m s^{-1}) in hist-aer (AER, blue), hist-GHG (GHG, green) and hist-nat (NAT, purple) simulations from eight CMIP6 models (**a**-**h**) and their MME (**i**) during 1900-2020. Linear trends of SWS (units: m s^{-1} per decade) in the observations (red) and in AER (blue), GHG (green), and NAT (purple) simulations from CMIP6 MME during 1980-2010 (**j**) and 2010-2020 (**k**) based on the multiple linear regression model. The error bars denote the 95% confidence levels of simulated regional mean trends. Each variable is calculated as a regional average for the study area (38.5°-54°N, 119.5°-135°E).

3.4. Projected changes in SWS in the 21st century

To analyze the future changes in SWS over Northeast China, we use the MMEs from CMIP6 projections under four different emission scenarios. First, the evolution and trends of SWS for the historical and future projections over 1980-2100 are shown in Figure 5a. In general, SWS is predicted to continue the historical decreasing trend under all four scenarios, with more rapid decline under the higher emission scenarios (SSP3-7.0 and SSP5-8.5). This is the same as the above result that GHG can lead to weakened wind speeds. Specially, SWS decreases most sharply under the SSP3-7.0 scenario rather than the highest GHG emission scenario (SSP5-8.5). This is mainly attributed to the fact that the SSP3-7.0 scenario represents much higher aerosol emissions than the other three scenarios, mainly consisting of black carbon aerosols and sulfate aerosols (Chen *et al* 2020, Riahi *et al* 2016). The decreasing trends in SWS reach -0.0246 m s^{-1} per decade ($P < 0.01$) and -0.0185 m s^{-1} per decade ($P < 0.001$) in the mid-term and long-term periods, respectively (Figure 5b). Figures 5c-5j display the spatial patterns of SWS trend over the mid-term (2021–2060) and long-term (2061-2100) future period under different scenarios. For the SSP1-2.6 scenario, SWS decreases slightly in the mid-term and increases in the long-term, mainly owing to the lowest GHG emissions and aerosol emissions under this scenario. Under the SSP3-7.0 scenario, it shows a significant decline in SWS over most of Northeast China. However, under the SSP5-8.5 scenario, which has the highest GHG emissions, SWS declines slightly in the future because the contribution of GHG emissions to wind speeds is weak, consistent with the above findings.

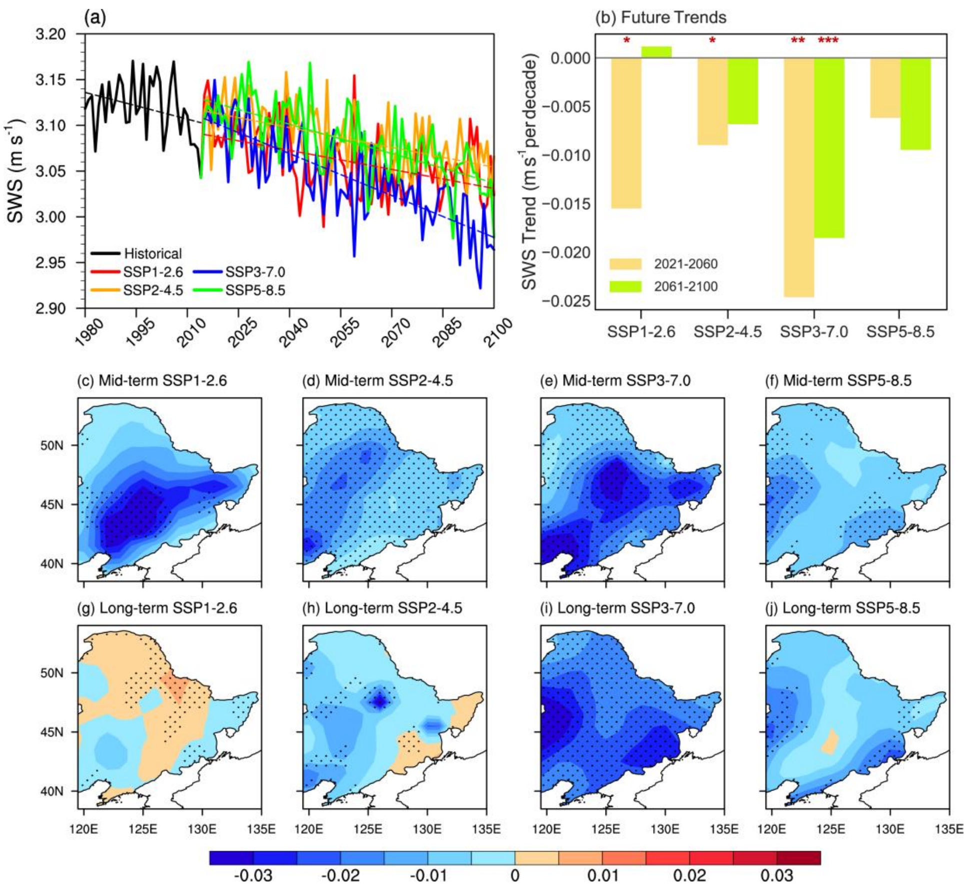

Figure 5. (**a**) Time series and linear trends of historical and projected SWS (units: m s^{-1}) under different scenarios during 1980-2100. (**b**) Projected trends of SWS for mid-term (2021-2060) and long-term (2061-2100) under different scenarios (units: m s^{-1} per decade). *, **, and *** indicate the trends passing 0.10, 0.01, and 0.001 significance levels, respectively. Blank denotes a trend is not significant. Spatial patterns of SWS

trend (units: m s^{-1} per decade) for mid-term (2021-2060, **c**-**f**) and long-term (2061-2100, **g**-**j**) future over Northeast China under SSP1-2.6 (**c** and **g**), SSP2-4.5 (**d** and **h**), SSP3-7.0 (**e** and **i**), and SSP5-8.5 (**f** and **j**). Stippling indicates the region where more than 5 out of the 7 CMIP6 models agree on the sign of the trends.

4. Conclusions and discussion

We provide a comprehensive analysis of the long-term trend change in SWS over Northeast China and the factors that contribute to the SWS reversal after 2010. The interdecadal variations of both annual and seasonal mean SWS exhibit a decline during 1980-2010, followed by an increasing trend after 2010, which are linked to the interdecadal transition of aerosol emissions. The AOD peaks in 2010 and then declines rapidly, showing a significant negative correlation with SWS, especially for the annual mean and for spring and summer seasons. The connection between AOD and SWS is modulated by aerosols via influencing the lower-level static stability. The reduction of aerosols contributes to the development of instability and promotes the growth of TKE, which in turn enhances SWS. The result is verified by multiple single forcing experiments in the DAMIP. In the aerosol-only forcing experiment, the SWS decreases accompanied by the increasing AOD and surface static stability from 1970 to 2010 and strengthens after 2010 due to decreasing aerosol emissions. The decrease in SWS from 1970 to 2010 is attributed to a combined effect of aerosol and greenhouse warming, with a stronger impact from the former. The contribution of natural forcing to the change of SWS trend during 1900-2020 is not obvious. By quantitative estimate, the change in observed SWS trends from 1980 to 2020 is mainly attributed to aerosol changes. As a result, the reduction of AOD primarily leads to the reversal of SWS in Northeast China. Future projections show continued declines in SWS under four scenarios, particularly under the SSP3-7.0 scenario, which represents the highest aerosol emissions. These findings indicate the importance of reducing aerosol emissions, which has a crucial role in mitigating the energy crisis and sustainable development of human society.

The local effects of aerosols are highlighted in this paper, i.e., aerosol radiation effects alter the thermodynamic stability and convective potential of the lower atmosphere, leading to lower temperatures and weaker winds in the lower atmosphere due to increased atmospheric stability. The stabilization of atmosphere affects turbulence and vertical transport of horizontal momentum, leading to differences of wind changes at high and low altitudes, which in turn affect the local circulation. In addition, on the continental scale, aerosols absorb solar radiation and cool the surface, reducing the land-ocean thermal contrast to suppress the monsoon development (Lau *et al* 2016). The Asian monsoon region is a major source of emissions of various aerosols, thus, the reduction of SWS under aerosol forcing is more intense in East Asia and South Asia than in the other regions (Li *et al* 2016). As a result, the influences of aerosols on the monsoon circulation and on SWS are closely related; and the physical mechanisms by which aerosols affect the monsoon and SWS are complex and should be investigated more systematically in the future. Note that GHG warming is also found to trigger the SWS trend in Figure 4, which appears to be through its modulation of the meridional atmospheric circulation (Deng *et al* 2021).

Yang *et al* (2021) performed a quantitative analysis of the SWS transition in China and found obvious regional differences. The years with annual and seasonal mean SWS from weakening to strengthening are around 1993/1994 and 2000 in Western Xinjiang and the Tibetan Plateau, while the terrestrial stilling is continuously ongoing and no reversal has occurred in North China, Eastern Xinjiang, and the eastern and southern coastal areas. The variation in SWS reflects a complicated physical process influenced by both internal climate variability and human activities. Moreover, the interactions and moderating effects among different internal variabilities are evident. Therefore, the changes in SWS should be determined by the combined effect of multiple internal variabilities, rather than being simply linked to only one internal variability (Zha *et al* 2021b). Different dominant factors at different spatiotemporal scales should be further examined and identified in the future.

Data availability statement

Observational surface wind speeds used in this study from the daily dataset of basic meteorological elements of China's national ground meteorological stations (V3.0) can be obtained at http://data.cma.cn/data/cdcdetail/dataCode/A.0012.0001.html supported by the China Meteorological Data Service Center. The MERRA-2 dataset is from the National Aeronautics and Space Administration Goddard Space Flight Center (NASA/GSFC): https://disc.gsfc.nasa.gov/datasets?project=MERRA-2. The ERA-5 reanalysis data is available at https://cds.climate.copernicus.eu/cdsapp#!/dataset/reanalysis-era5-single-levels-monthly-means?tab=form from the European Centre for Medium-Range Weather Forecasts (ECMWF). The JRA-55 dataset is at https://jra.kishou.go.jp/JRA-55/index_en.html from the Japan Meteorological Agency (JMA). The CFSR data is acquired from the NCAR Research Data Archive (RDA) (https://rda.ucar.edu/datasets/ds093.0/dataaccess/#). The CMIP6 outputs used in this study can be downloaded from https://esgf-node.llnl.gov/projects/cmip6/.

Acknowledgements

This work is supported by the National Natural Science Foundation of China (42192562 and 41975106). We thank the High Performance Computing Center of Nanjing University of Information Science & Technology for supporting this research. Gratitude is extended to all the institutions for providing the relevant data used in this study.

References

Bao Z, Wen Z and Wu R 2009 Variability of aerosol optical depth over east Asia and its possible impacts *Journal of Geophysical Research: Atmospheres.* **114** D5. https://doi.org/10.1029/2008JD010603

Bichet A, Wild M, Folini D and Schär C 2012 Causes for decadal variations of wind speed over land: Sensitivity studies with a global climate model *Geophysical Research Letters.* **39** L11701. https://doi.org/10.1029/2012GL051685

Bluestein H B 1992 Synoptic-Dynamic Meteorology in Midlatitudes. Oxford University Press, 276 pp.

Chen Y, Liu A and Cheng X 2020 Quantifying economic impacts of climate change under nine future emission scenarios within CMIP6 *Science of the total environment.* **703** 134950. https://doi.org/10.1016/j.scitotenv.2019.134950

Deng K, Azorin-Molina C, Minola L, Zhang G and Chen D 2021 Global near-surface wind speed changes over the last decades revealed by reanalyses and CMIP6 model simulations *Journal of Climate.* **34** 2219-2234. https://doi.org/10.1175/JCLI-D-20-0310.1

Ding A J, et al 2016 Enhanced haze pollution by black carbon in megacities in China *Geophysical Research Letters.* **43** 2873-2879. https://doi.org/10.1002/2016GL067745

Ge J, Feng D, You Q, Zhang W and Zhang Y 2021 Characteristics and causes of surface wind speed variations in Northwest China from 1979 to 2019 *Atmospheric Research.* **254** 105527. https://doi.org/10.1016/j.atmosres.2021.105527

Gelaro R, et al 2017 The modern-era retrospective analysis for research and applications, version 2 (MERRA-2) *Journal of climate.* **30** 5419-5454. https://doi.org/10.1175/JCLI-D-16-0758.1

Gillett N P, Shiogama H, Funke B, Hegerl G, Knutti R, Matthes K, Santer B D, Stone D and Tebaldi C 2016 Detection and Attribution Model Intercomparison Project (DAMIP) *Geoscientific Model Development.* **9** 3685-3697. https://doi.org/10.5194/gmd-2016-74

Grabowski W W, Wang L P and Prabha T V 2015 Macroscopic impacts of cloud and precipitation processes on maritime shallow convection as simulated by a large eddy simulation model with bin microphysics *Atmospheric Chemistry and Physics.* **15** 913-926. https://doi.org/10.5194/acp-15-913-2015

Guo H, Xu M and Hu Q 2011 Changes in near-surface wind speed in China: 1969-2005 *International Journal of Climatology.* **31** 349-358. https://doi.org/10.1002/joc.2091

He Q, Li C, Geng F, Lei Y and Li Y 2012 Study on long-term aerosol distribution over the land of East China using MODIS data *Aerosol and Air Quality Research.* **12** 304-319. https://doi.org/10.5194/acpd-11-10485-2011

Hersbach H, et al 2020 The ERA5 global reanalysis *Quarterly Journal of the Royal Meteorological Society.* **146** 1999-2049. https://doi.org/10.1002/qj.3803

Jacobson M Z and Kaufman Y J 2006 Wind reduction by aerosol particles *Geophysical Research Letters.* **33** L24814. https://doi.org/10.1029/2006GL027838

Jiang H, Feingold G and Cotton W R 2002 Simulations of aerosol-cloud-dynamical feedbacks resulting from entrainment of aerosol into the marine boundary layer during the Atlantic Stratocumulus Transition Experiment *Journal of Geophysical Research: Atmospheres.* **107** 24. https://doi.org/10.1029/2001JD001502

Jiang Q, Li W, Fan Z, He X, Sun W, Chen S, Wen J, Gao J and Wang J 2021 Evaluation of the ERA5 reanalysis precipitation dataset over Chinese Mainland *Journal of hydrology.* **595** 125660. https://doi.org/10.1016/j.jhydrol.2020.125660

Kim S W, Yoon S C, Kim J and Kim S Y 2007 Seasonal and monthly variations of columnar aerosol optical properties over east Asia determined from multi-year MODIS, LIDAR, and AERONET Sun/sky radiometer measurements *Atmospheric Environment.* **41** 1634-1651. https://doi.org/10.1016/j.atmosenv.2006.10.044

Kobayashi S, et al 2015 The JRA-55 reanalysis: General specifications and basic characteristics *Journal of the Meteorological Society of Japan. Ser. II.* **93** 5-48. https://doi.org/10.2151/jmsj.2015-001

Lau W K 2016 The aerosol-monsoon climate system of Asia: A new paradigm *Journal of Meteorological Research.* **30** 1-11. https://doi.org/10.1007/s13351-015-5999-1

Li X, Li Q P, Ding Y H and Wang M 2022 Near-surface wind speed changes in eastern China during 1970–2019 winter and its possible causes *Advances in Climate Change Research.* **13** 228-239. https://doi.org/10.1016/j.accre.2022.01.003

Li Z, Niu F, Fan J, Liu Y, Rosenfeld D and Ding Y 2011 Long-term impacts of aerosols on the vertical development of clouds and precipitation *Nature Geoscience.* **4** 888-894. https://doi.org/10.1038/ngeo1313

Li Z, et al 2016 Aerosol and monsoon climate interactions over Asia *Reviews of geophysics.* **54** 866-929. https://doi.org/10.1002/2015RG000500

Lin C, Yang K, Qin J and Fu R 2013 Observed coherent trends of surface and upper-air wind speed over China since 1960 *Journal of Climate.* **26** 2891-2903. https://doi.org/10.1175/JCLI-D-12-00093.1

Miao H, Dong D, Huang G, Hu K, Tian Q and Gong Y 2020 Evaluation of Northern Hemisphere surface wind speed and wind power density in multiple reanalysis datasets *Energy.* **200** 117382. https://doi.org/10.1016/j.energy.2020.117382

Miao H, Xu H, Huang G and Yang K 2023 Evaluation and future projections of wind energy resources over the Northern Hemisphere in CMIP5 and CMIP6 models *Renewable Energy.* **211** 809-821. https://doi.org/10.1016/j.renene.2023.05.007

Moreira E E, Martins D S and Pereira L S 2015 Assessing drought cycles in SPI time series using a Fourier analysis *Natural Hazards and Earth System Sciences.* **15** 571-585. https://doi.org/10.5194/nhess-15-571-2015

O'Neill B C, et al 2016 The scenario model intercomparison project (ScenarioMIP) for CMIP6 *Geoscientific Model Development.* **9** 3461-3482. https://doi.org/10.5194/gmd-9-3461-2016

Pettitt A N 1979 A non-parametric approach to the change-point problem *Journal of the Royal Statistical Society: Series C (Applied Statistics).* **28** 126-135. https://doi.org/10.2307/2346729

Riahi K, et al 2017 The Shared Socioeconomic Pathways and their energy, land use, and greenhouse gas emissions implications: An overview *Global environmental change.* **42** 153-168. https://doi.org/10.1016/j.gloenvcha.2016.05.009

Saha S, et al 2010 The NCEP climate forecast system reanalysis *Bulletin of the American Meteorological Society.* **91** 1015-1058. https://doi.org/10.1175/2010BAMS3001.1

Schaefer D and Domroes M 2009 Recent climate change in Japan-spatial and temporal characteristics of trends of temperature *Climate of the Past.* **5** 13-19. https://doi.org/10.5194/cp-5-13-2009

Sen P K 1968 Estimates of the regression coefficient based on Kendall's tau *Journal of the American statistical association.* **63** 1379-1389. https://doi.org/10.1080/01621459.1968.10480934

Shen C, Zha J, Zhao D, Wu J, Fan W, Yang M and Li Z 2021 Estimating centennial-scale changes in global terrestrial near-surface wind speed based on CMIP6 GCMs *Environmental Research Letters.* **16** 084039. https://doi.org/10.1088/1748-9326/ac1378

Su T, Feng T and Feng G 2015 Evaporation variability under climate warming in five reanalyses and its association with pan evaporation over China *Journal of Geophysical Research: Atmospheres.* **120** 8080-8098. https://doi.org/10.1002/2014JD023040

Tariq S, Qayyum F, Ul-Haq Z and Mehmood U 2022 Long-term spatiotemporal trends in aerosol optical depth and its relationship with enhanced vegetation index and meteorological parameters over South Asia *Environmental Science and Pollution Research.* **29** 30638-55. https://doi.org/10.1007/s11356-021-17887-4

Tian Q, Huang G, Hu K and Niyogi D 2019 Observed and global climate model based changes in wind power potential over the Northern Hemisphere during 1979-2016 *Energy.* **167** 1224-1235. https://doi.org/10.1016/j.energy.2018.11.027

Vautard R, Cattiaux J, Yiou P, Thépaut J N and Ciais P 2010 Northern Hemisphere atmospheric stilling partly attributed to an increase in surface roughness *Nature geoscience.* **3** 756-761. https://doi.org/10.1038/ngeo979

Xu M, Chang C P, Fu C, Qi Y, Robock A, Robinson D and Zhang H M 2006 Steady decline of east Asian monsoon winds, 1969-2000: Evidence from direct ground measurements of wind speed *Journal of Geophysical Research: Atmospheres.* **111** D24 https://doi.org/10.1029/2006JD007337

Yang Q, Li M, Zu Z and Ma Z 2021 Has the stilling of the surface wind speed ended in China? *Science China Earth Sciences.* **64** 1036-1049. https://doi.org/10.1007/s11430-020-9738-4

Yang X, Li Z, Feng Q, He Y, An W, Zhang W, Cao W, Yu T, Wang Y and Wilfred H T 2012 The decreasing wind speed in southwestern China during 1969-2009, and possible causes *Quaternary International.* **263** 71-84. https://doi.org/10.1016/j.quaint.2012.02.020

Yang X, Ferrat M and Li Z 2013 New evidence of orographic precipitation suppression by aerosols in central China *Meteorology and Atmospheric Physics* **119** 17-29. https://doi.org/10.1007/s00703-012-0221-9

Yu H, Liu S C and Dickinson R E 2002 Radiative effects of aerosols on the evolution of the atmospheric boundary layer *Journal of Geophysical Research: Atmospheres.* **107** 4142. https://doi.org/10.1029/2001JD000754

Zeng Z, et al 2019 A reversal in global terrestrial stilling and its implications for wind energy production *Nature Climate Change.* **9** 979-985. https://doi.org/10.1038/s41558-019-0622-6

Zha J, Wu J and Zhao D 2017 Effects of land use and cover change on the near-surface wind speed over China in the last 30 years *Progress in Physical Geography.* **41** 46-67. https://doi.org/10.1177/0309133316663097

Zha J, Shen C, Li Z, Wu J, Zhao D, Fan W, Sun M, Azorin-Molina C and Deng K 2021a Projected changes in global terrestrial near-surface wind speed in 1.5°C-4.0°C global warming levels *Environmental Research Letters.* **16** 114016. https://doi.org/10.1088/1748-9326/ac2fdd

Zha J, Shen C, Zhao D, Wu J and Fan W 2021b Slowdown and reversal of terrestrial near-surface wind speed and its future changes over eastern China *Environmental Research Letters.* **16** 034028. https://doi.org/10.1088/1748-9326/abe2cd

Zhang G, Azorin-Molina C, Chen D, McVicar T R, Guijarro J A, Kong F, Minola L, Deng K and Shi 2021 Uneven warming likely contributed to declining near-surface wind speeds in northern China between 1961 and 2016 *Journal of Geophysical Research: Atmospheres.* **126** e2020JD033637. https://doi.org/10.1029/2020JD033637

Zhang J, Ren G and You Q 2024 Detection and attribution of human-perceived warming over China *Geophysical Research Letters.* **51** e2023GL106283. https://doi.org/10.1029/2023GL106283

Zhang Z and Wang K 2020 Stilling and recovery of the surface wind speed based on observation, reanalysis, and geostrophic wind theory over China from 1960 to 2017 *Journal of Climate.* **33** 3989-4008. https://doi.org/10.1175/JCLI-D-19-0281.1